



**HAL**  
open science

## Impact of Metal Content on the Deactivation of a Bifunctional Hydrocracking Catalyst

July Vivas-Báez, Gerhard Pirngruber, Alberto Servia, Anne-Claire Dubreuil,  
David Pérez-Martínez

► **To cite this version:**

July Vivas-Báez, Gerhard Pirngruber, Alberto Servia, Anne-Claire Dubreuil, David Pérez-Martínez. Impact of Metal Content on the Deactivation of a Bifunctional Hydrocracking Catalyst. *Energy & Fuels*, 2022, 36 (8), pp.4491-4501. 10.1021/acs.energyfuels.1c04384 . hal-03779128

**HAL Id: hal-03779128**

**<https://ifp.hal.science/hal-03779128>**

Submitted on 16 Sep 2022

**HAL** is a multi-disciplinary open access archive for the deposit and dissemination of scientific research documents, whether they are published or not. The documents may come from teaching and research institutions in France or abroad, or from public or private research centers.

L'archive ouverte pluridisciplinaire **HAL**, est destinée au dépôt et à la diffusion de documents scientifiques de niveau recherche, publiés ou non, émanant des établissements d'enseignement et de recherche français ou étrangers, des laboratoires publics ou privés.

# IMPACT OF METAL CONTENT ON THE DEACTIVATION OF A BIFUNCTIONAL HYDROCRACKING CATALYST

July C. VIVAS-BÁEZ<sup>a</sup>, Gerhard D. PIRNGRUBER<sup>a,\*</sup>, Alberto SERVIA<sup>a</sup>, Anne-Claire DUBREUIL<sup>a</sup>, David J. PÉREZ-MARTÍNEZ<sup>b</sup>

*a IFP Energies nouvelles, Rond-point de l'échangeur de Solaize, France, 69360.*

*b Centro de innovación y tecnología ICP, ECOPETROL S.A., Km 7 vía Piedecuesta, Piedecuesta, Colombia, 681011.*

Corresponding Author: Gerhard PIRNGRUBER (<mailto:gerhard.pirngruber@ifpen.fr>)

**Keywords:** deactivation, bifunctional catalyst, metal/acid balance, nitrogen poisoning, hydrocracking.

## ABSTRACT

The catalytic performance of a hydrocracking bifunctional catalyst and, consequently, its activity loss depends on the balance between the metal (M) and acid (A) functions. Commonly, the metal function is reputed to stabilize catalyst activity and should, therefore, alleviate deactivation. In order to test this hypothesis, this study aimed to assess the impact of the metal oxide (MoO<sub>3</sub>) content on the deactivation of a vacuum gasoil hydrocracking catalyst (a nickel-molybdenum sulfide dispersed on a carrier containing USY zeolite). To do so, two bifunctional catalysts with different metal oxide contents were submitted to specific operating conditions promoting catalysts deactivation, i.e., high temperature (T=418°C) and high space velocity (LHSV=3 h<sup>-1</sup>). Experiments were carried out in a pilot unit with a hydrotreated VGO feedstock containing 120 ppmw of organic nitrogen. The loss in activity was measured by following the decrease of both the VGO conversion (370°C<sup>+</sup>) and the apparent kinetic constants for the main hydrocracking reactions (cracking, hydrodenitrogenation and aromatics hydrogenation) with time on stream. The aged catalysts, sampled from three different reactor locations, were characterized by elemental, textural analysis and thermogravimetry to investigate the quantity and nature of the coke deposits. To determine

28 the residual activity of the hydrogenation and acid catalyst functions, catalytic tests with different  
29 model compounds (toluene and n-heptane) were carried out. It was observed that in the  
30 hydrocracking of feedstocks with high nitrogen concentration, the decrease of the metal content  
31 causes a substantial increase of the nitrogen compounds concentration in the catalytic bed. This  
32 increase significantly reduces the available acid sites and, hence, the hydrocracking activity. But  
33 at the same time, the M/A ratio is modified in favor of the metal function. The better balance of the  
34 catalyst with low metal loading results in a lower coke deposition and, consequently, a lower  
35 deactivation rate than with the catalyst with higher metal content.

## 36 **1 INTRODUCTION**

37 The hydrocracking of vacuum gasoils (VGO) is a refining process to produce mainly middle  
38 distillates (diesel and kerosene) <sup>1-3</sup>. This process employs bifunctional heterogeneous catalysts  
39 that combine a (de)/hydrogenation and an acid function. Commonly the (de)/hydrogenation  
40 function is provided by metal sulfides from group VIA (molybdenum, tungsten) and group VIIIA  
41 (nickel) <sup>4-6</sup>. Ultra-stable Y zeolites are widely used as acid components in hydrocracking catalysts  
42 <sup>7</sup>. In the classical bifunctional hydrocracking mechanism <sup>8-11</sup>, the metal function serves to  
43 dehydrogenate alkanes to the corresponding alkenes. These alkenes are desorbed from the metal  
44 sites and diffuse to the acid sites, where they are protonated to carbenium ions. These  
45 carbocations undergo skeletal isomerization and cracking; their products are desorbed as alkenes  
46 which are finally hydrogenated to alkanes on metal sites. Thus, catalyst activity, stability and  
47 selectivity strongly depend on the balance between the metal and acid functions (M/A) <sup>12-14</sup>, the  
48 distance between these functions (Weisz's intimacy criterion) <sup>9,11,15</sup> and on the characteristics of  
49 the zeolite pores <sup>15,16</sup>.

50 Several authors have studied the balance between the metal and acid functions (M/A). For  
51 bifunctional catalysts based on a noble metal (Pt) during the hydroisomerization and

52 hydrocracking reactions of n-heptane <sup>13,14</sup> and n-decane <sup>17</sup>, Guisnet et al. <sup>13,14,17,18</sup> found that at  
53 low (M/A) ratios, the initial activity per acid site is low and increases with the increase of this ratio  
54 until reaching a stable value, which corresponds to a bifunctional mechanism limited by the acid  
55 sites. They also found that at low M/A ratio, the catalyst stability is poor because there is a fast  
56 coke formation. For high M/A values, the catalyst is well balanced (i.e., acid-catalyzed reactions  
57 become the limiting step <sup>19</sup>) and the reaction follows the well-known ideal bifunctional  
58 hydrocracking mechanism. Other works <sup>20,21</sup> also confirmed the relation between the metal loading  
59 and catalyst activity. Degnan and Kennedy <sup>21</sup> evaluated the hydroisomerization of n-heptane on a  
60 Pt catalyst and they found that an imbalance between the hydrogenation and the acid functions  
61 can even alter the apparent reaction network of the system. Denayer et al. <sup>22</sup> found a reduction in  
62 activity with an increase of the (M/A) obtained by reducing the number of acid sites. The reduction  
63 in activity is related to the decrease in acidity and consequently in cracking power.

64 For metal sulfide catalysts, Mendes et al. <sup>23</sup> quantified the amount of Brönsted acid sites available  
65 in an ammonia atmosphere during the hydroconversion of cyclohexane and found that just around  
66 1% of the acid sites remained available in the presence of ammonia. They noted that for two well-  
67 balanced NiMo catalysts with different Mo content, there is no difference in activity or selectivity  
68 independently of the ammonia content. Pirngruber et al. <sup>19</sup> compared the performance of metal  
69 sulfided catalysts with different acidity levels on the hydroconversion of n-hexadecane. They found  
70 that the inhibition of the acid sites by ammonia, in association with low zeolite contents, is  
71 necessary to balance NiMo sulfide hydrocracking catalysts. They also observed a negative  
72 correlation between catalyst selectivity to isomerization reactions and zeolite loading. The impact  
73 of MoO<sub>3</sub> loading on activity was quite small because it was mainly governed by the zeolite loading  
74 of the catalysts. In a similar work, Mendes et al. <sup>24</sup> confirm that ammonia helps to equilibrate the  
75 metal-acid balance in NiMo catalysts. They also evaluated catalysts with different molybdenum  
76 loadings in the n-hexadecane hydroconversion, but no noticeable evolution of the activity with Mo

77 loading and only a minor evolution of the maximal C16 isomer yield were observed. M.V.  
78 Bukhtiyarova et al.<sup>25</sup> studied the effect of sulfosalicylic acid treatment on the properties of Beta  
79 zeolite (BEA and BEA-SA) and the performance of NiW/Beta-Al<sub>2</sub>O<sub>3</sub> catalysts in hexadecane  
80 hydrocracking. The total Brønsted and Lewis acid sites concentration decreased with an acid  
81 treatment and as a result, the metal-acid balance of the catalyst shifted towards enhanced metal  
82 function, providing the beneficial effect on hexadecane hydrocracking selectivity. I.G. Danilova et  
83 al.<sup>26</sup> worked on the impact of rare earths on the acidity of high-silica ultrastable REY zeolites and  
84 catalytic performance of NiMo/REY+Al<sub>2</sub>O<sub>3</sub> catalysts in VGO hydrocracking; they found that the  
85 increase in RE<sub>2</sub>O<sub>3</sub> content led to a decrease in the strong acid site density, which suppresses  
86 overcracking reactions and improves the selectivity to middle distillates.

87 The deactivation of bifunctional hydrocracking catalysts with VGO feeds is dominated by the  
88 poisoning involving organic nitrogen compounds and coke deposition <sup>27–29</sup>. N-compounds are  
89 strongly adsorbed on the catalyst surface compared with other hydrocarbon structures present in  
90 the feed <sup>30–32</sup>. With a longer time on stream, the adsorbed species are converted to coke <sup>33–37</sup>.  
91 Concerning deactivation by coke, two different mechanisms have been proposed to explain coke  
92 formation on the metal and the acid sites of bifunctional catalysts. On metal sites, it is presumed  
93 that coke results from successive dehydrogenation reactions leading to atomic carbon or partially  
94 hydrogenated intermediates that combine to form a graphitic coke <sup>38,39</sup>. On acid sites, it is accepted  
95 that coke results from the polymerization of dehydrogenated intermediates generated on the metal  
96 sites <sup>40</sup>.

97 The deactivation of bifunctional catalysts by coking has been the subject of numerous  
98 investigations. Many of these studies were carried out on reforming catalysts, having a  
99 hydrogenation–dehydrogenation function (Pt or Pt-Re) and an acid function (Al<sub>2</sub>O<sub>3</sub> or chlorinated  
100 Al<sub>2</sub>O<sub>3</sub>). Barbier <sup>40</sup> analyzed the deposited coke on a spent reforming catalyst by temperature-  
101 programmed combustion and identified the presence of two peaks, one at around 300°C and the

102 other at around 450°C. It was established that the low-temperature (300°C) combustion was due  
103 to the presence of coke on the metal phase. The results of Barbier determined that the amount of  
104 coke deposited on the metallic function of a bifunctional catalyst always corresponded to a small  
105 fraction of the amount of coke accumulated in the whole catalyst. Querini et al.<sup>41</sup> also analyzed  
106 some industrial reforming catalyst, Pt/Al<sub>2</sub>O<sub>3</sub>, by thermal programmed oxidation (TPO) and found  
107 that coke is deposited first on the metal and then on the acid sites. Coke on metal increases with  
108 time initially and then remains constant, while coke on the acid sites increases during the whole  
109 run. The coke deposited on the metal is more dehydrogenated than the coke deposited on the  
110 support<sup>42</sup>. Bartholomew<sup>30</sup> claimed that in the coke deactivation of reforming catalysts, coke  
111 precursors might be formed on the metal sites via hydrogenolysis.

112 Most studies on the effect of the metal/acid sites ratio have been carried out using platinum  
113 catalysts. In contrast, there is not much work with metal sulfide catalysts. To the best of our  
114 knowledge, they all use different model molecules, especially alkanes, to evaluate the  
115 hydroconversion reactions under conditions, not representative of the industrial process and  
116 where there is no catalyst deactivation. Therefore, this work aims to evaluate the impact of  
117 Molybdenum loading on the deactivation of a NiMo hydrocracking catalyst using a real feed.  
118 Therefore, two bifunctional catalysts with different metal oxide contents were submitted to specific  
119 operating conditions promoting catalysts deactivation in a pilot unit with a hydrotreated VGO,  
120 according to the accelerated deactivation protocol developed in our previous work<sup>43</sup>.

## 121 **2 EXPERIMENTAL SECTION**

### 122 **2.1 Feedstock**

123 The feedstock was a hydrotreated blend of 71% vacuum gasoil, 16% coker gasoil and 13% light  
124 cycle oil on a weight basis. The main properties of this feed are shown in

125 Table 1. Dimethyl disulfide and aniline were added to the hydrotreated VGO to generate the  
126 hydrogen sulfide and ammonia partial pressures representative of the VGO mother feed. The  
127 mother feed contained a sulfur and a nitrogen content of 1.18 and 0.25 wt%, respectively.

128

**Table 1. Feedstock properties.**

<b>Properties</b>		<b>Feed</b>
Density @ 15°C	g/cm <sup>3</sup>	0.8679
Refraction Index @ 70° C		1.4791
Sulfur	wt%	0.016
Nitrogen	ppmw	120
Aromatics content	wt%	~42
Yield of 370°C+ fraction	wt%	64
Initial boiling point (IBP)	°C	131
T50 Boiling point	°C	397
Final boiling point (FBP)	°C	554

129

## 130 **2.2 Catalysts**

131 The reference catalyst consists of nickel-molybdenum sulfide particles dispersed on a carrier  
132 containing USY zeolite. A series of catalysts with varying metal oxide content at a constant Ni/Mo  
133 molar ratio was prepared to evaluate the impact of molybdenum content. Their molybdenum oxide  
134 contents were 25%, 50% and 75% of the molybdenum oxide content related to the reference  
135 catalyst. No modification was made to the zeolitic support. These fresh catalysts were used to  
136 determine the activity of each function at different metal oxide contents. Based on these results,  
137 the catalyst with 50% molybdenum was chosen to be subjected to the accelerated deactivation  
138 conditions developed in our previous work <sup>43</sup> and compare its performance with that of the  
139 reference catalyst.

140 The catalysts were synthesized by incipient wetness impregnation of the zeolitic support in  
141 extrudates shape with a solution containing Ni and Mo precursors. After 1.5 hours of maturation,

142 the solids were dried at 120°C for 12 hours and then calcined at 450 °C for 2 hours under air. No  
143 additional information on catalyst properties is given for confidentiality reasons.

### 144 **2.3 Experimental set-up**

145 The test runs were conducted in an up-flow fixed-bed pilot unit. Detailed information has been  
146 reported elsewhere <sup>43</sup>. The pilot plant comprised two isothermal reactors in series, loaded with the  
147 same hydrocracking catalyst diluted with inert carborundum (SiC). Thus, both reactors operate on  
148 hydrocracking reactions. The unit has a liquid sampling system between the two reactors. The gas  
149 and liquid phases from the total effluent were separated by a high-pressure separator installed  
150 downstream of the second reactor. The gaseous effluent was transferred to a gas flow meter and  
151 then analyzed online by gas chromatography, while the liquid product was sent to a stripper and  
152 finally to a storage vessel. The liquid products were characterized by density, refractive index,  
153 nitrogen and sulfur contents and simulated distillation to daily track catalyst performance.

### 154 **2.4 Experimental procedure**

155 At the beginning of the pilot unit tests, the catalyst was sulfided in situ with an atmospheric gasoil  
156 spiked with 2% wt. (%/feed) of dimethyl disulfide (DMDS) and 2% wt. aniline (%/feed) at 350°C  
157 and 14MPa. After this step, the deactivation conditions were imposed, i.e., 418°C, LHSV of 3 h<sup>-1</sup>,  
158 H<sub>2</sub>/HC = 1500 NL/L and P = 14 MPa, with the feedstock described in section 2.1. The catalyst  
159 remained at the same conditions for 30 days. The density of the liquid effluent tracked the  
160 stabilization of the catalyst. The performance was considered stable when the density variation  
161 was lower than 0.0010 g/cm<sup>3</sup> for 24 consecutive hours. However, in those tests, the catalyst  
162 immediately went into a deactivation regime at the conditions applied, barely showing stabilization.  
163 Therefore, in the evaluation of the experimental results, the experimental points from the first two  
164 days were not considered because the effects of the system stabilization and catalyst deactivation  
165 can be superimposed at the beginning of the test. The unit was washed with atmospheric gasoil  
166 at the end of the experiment. The catalyst was stripped and dried with hydrogen before being



167 unloaded. Catalyst samples taken at the end of each experiment were carefully collected to  
168 separate the particles from the inlet, middle and outlet of each catalytic bed. More information  
169 about specific experimental procedures can be found elsewhere <sup>43</sup>.

## 170 **2.5 Kinetic performance evaluation**

171 The conversion of VGO (370°C<sup>+</sup>) (Equation 1) was monitored to assess the catalytic performance.  
172 However, interpreting the raw conversion data can be misleading, especially when the conversion  
173 is high. As the conversion increases, the reactant is depleted. Consequently, the differential  
174 reaction rate decreases. A kinetic model must be established to do a rigorous analysis of reaction  
175 rates, but for the complex reaction network of the VGO, this requires a significant amount of input  
176 data <sup>43</sup>, which was not available in our case. Therefore, for simplicity's sake, power-law models  
177 were used to calculate the apparent kinetic constants for the main reactions (cracking,  
178 hydrodenitrogenation-HDN and aromatics hydrogenation-HDA). The inhibition and deactivation  
179 were followed by the change in these constants during time on stream. The aim was to compare  
180 the different reaction rates for the two selected catalysts. A first-order <sup>43</sup> kinetics was assumed for  
181 both N-containing and aromatic molecules <sup>43</sup> (Equation 2), i.e., for HDN and HDA, respectively.  
182 To determine the apparent HDA kinetic constant, the amount of aromatic carbon was estimated  
183 through the n-d-M method according to the standard ASTM D3238.

$$\% \text{Net Conversion} = \left( \frac{\text{mass}_{x \text{ feed}} - \text{mass}_{x \text{ product}}}{\text{mass}_{x \text{ feed}}} \right) * 100 \quad \text{Equation 1}$$

Where x is either the 370<sup>+</sup> mass fraction, the nitrogen content or the aromatic carbon content.

$$k = \text{LHSV} * \ln(1 - \% \text{Net Conversion} / 100) \quad \text{Equation 2}$$

184 For reactions affected by catalyst deactivation, there is a dependence of the kinetic performance  
185 on deactivation. Therefore, an exponential decay model with three parameters (Equation 3) was  
186 assumed to dissociate both phenomena for cracking reactions. In this model, the catalyst  
187 deactivation depends on the deactivation constant and time on stream (TOS) <sup>43-45</sup>. The alpha ( $\alpha$ )

188 (1/time) parameter accounts for the activity loss rate by deactivation of the catalyst. Finally, the c  
189 parameter represents the residual activity of the spent catalysts.

$$k_{\text{crack}} = A \cdot \exp(-\alpha \cdot \text{TOS}) + c \quad \text{Equation 3}$$

190 (A+c) corresponds to the kinetic constant of the fresh catalyst at time = 0.

## 191 **2.6 Samples Characterization**

### 192 2.6.1 Liquid Samples Characterization

193 Feed and liquid products (sampled every day) were characterized by a densimeter for determining  
194 the density, by chemiluminescence for the nitrogen content, by X-Ray fluorescence spectrometry  
195 for the sulfur content and gas chromatography for the simulated distillation.

### 196 2.6.2 Catalyst Characterization

197 Before being characterized, the spent catalyst samples were submitted to extraction with toluene  
198 in a soxhlet extractor at 250°C for 7 h and dried under vacuum at 120°C for 12 h. Then the following  
199 analyses were carried out. The carbon, hydrogen and nitrogen contents were determined on a  
200 Thermoscientific FlashSmart equipment. Nitrogen adsorption-desorption isotherms  
201 measurements were performed in an ASAP Micromeritics apparatus to determine the catalyst  
202 surface area and total pore volume. Additionally, the catalyst was analyzed by elemental  
203 thermogravimetry on a thermobalance Mettler Toledo TGA-DSC1 coupled with a mass  
204 spectrometer. The MoS<sub>2</sub> sheets were visualized and analyzed by transmission electron  
205 microscopy with a JEOL JEM 2100F microscope to determine the slab length and promotion. The  
206 TEM images were recorded in the bright field mode. The average dispersion of the MoS<sub>2</sub> particles  
207 was calculated from the slab length distribution, assuming a hexagonal shape for the particles<sup>46</sup>.  
208 Finally, the promotion degree of the MoS<sub>2</sub> particles was investigated by TEM-EDX detection,  
209 leading to Ni/Mo ratio calculated for about 25 particles.

### 210 2.6.3 Catalytic tests with model molecules

211 Catalytic tests with model compounds were carried out to characterize the activity of both catalytic  
212 functions for the fresh and the spent catalysts. The hydrogenation activity was evaluated by  
213 converting toluene to hydrogenated products. For fresh catalysts, the reaction was carried out in  
214 the presence of aniline (0.5 wt %) in order to moderate their activity. In the case of spent catalysts,  
215 no aniline was used. The cracking function was determined by the hydroconversion of n-heptane  
216 to isomerization and cracking products. The used methods are analogous to the one described  
217 elsewhere <sup>47</sup>. The catalytic tests were carried out in a high-throughput fixed bed reactor unit in the  
218 presence of H<sub>2</sub>S (generated by decomposition of DMDS) under hydrogen pressure. Catalysts  
219 samples were sulfided in situ. The operating conditions for each experiment are presented in Table  
220 2.

221 **Table 2. Operating conditions of the catalytic tests with model molecules.**

		Toluene Hydrogenation		n-Heptane Hydroconversion		
		Fresh catalyst	Spent catalyst	Fresh catalysts	and	spent
Concentration of reactant	wt %/feed	20*	20*			95.15
DMDS concentration	wt %/feed	6	6			4.85
Aniline concentration	wt %/feed	0.5	--		--	
P	MPa	6	6			6
LHSV	h <sup>-1</sup>	2	2			4
T	°C	350	350			350/360/380
H <sub>2</sub> /HC	NL/L	450	450			330

222 \*in cyclohexane as solvent

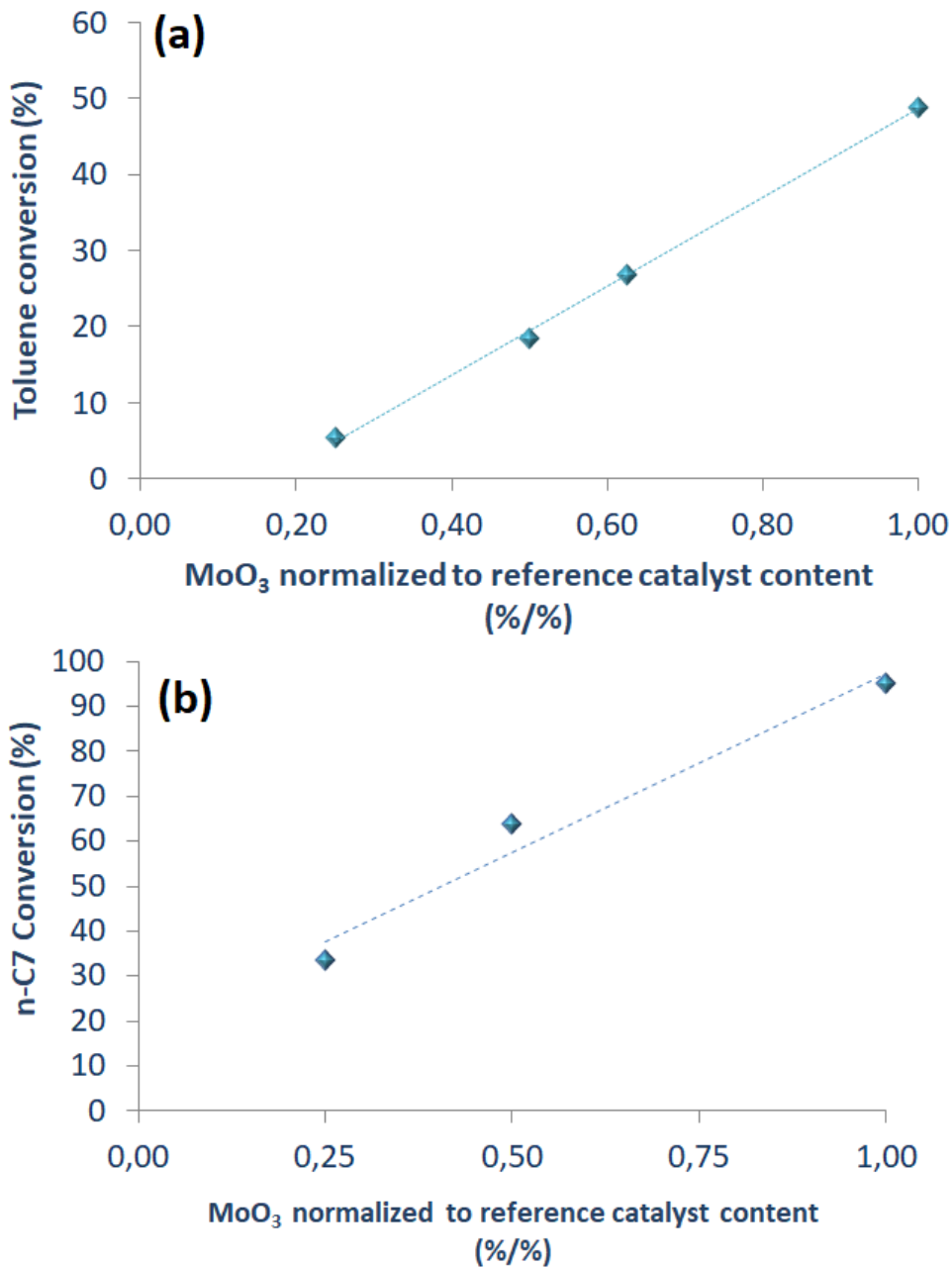
## 223 3 RESULTS

224 To evaluate the impact of the MoO<sub>3</sub> loading on catalyst performance, the results of the model  
225 molecule (Toluene, n-heptane) tests obtained with catalysts with different metal contents are firstly

226 presented. These results serve as a basis for the interpretation of the VGO hydrocracking  
227 experiments under deactivation conditions for two catalysts with different metal content, which are  
228 reported in section 3.2. Subsequently, the characterization of the spent catalysts obtained in the  
229 pilot plant tests is shown in section 3.3.

### 230 **3.1 Model molecules tests for fresh catalysts with different MoO<sub>3</sub> contents**

231  
232 In Figure 1a, the hydrogenation activity of the catalysts is presented as a function of their MoO<sub>3</sub>  
233 content; as expected, the conversion increased with the metal oxide content. Concerning the  
234 cracking function, the lower the amount of molybdenum, the lower the activity, although all  
235 catalysts had the same zeolite content (see Figure 1b). The strong dependence of the cracking  
236 activity on molybdenum loading is quite remarkable because it is more pronounced than reported  
237 in previous studies<sup>19,23,24</sup>. This indicates a strong limitation of the bifunctional mechanism by the  
238 initial dehydrogenation steps.

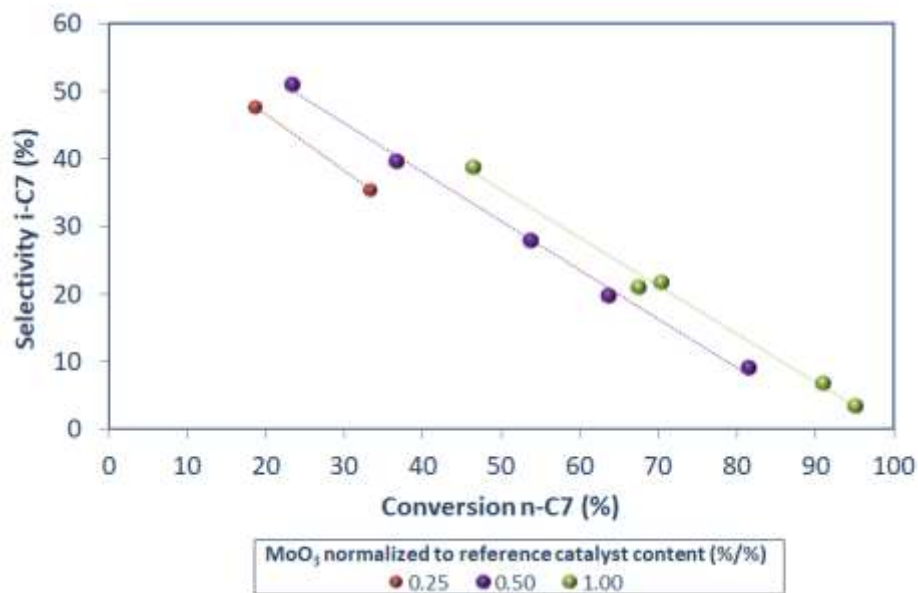


239

240 **Figure 1. Catalytic activities evaluated by model molecules catalytic tests for fresh, dried catalyst**  
 241 **samples with different MoO<sub>3</sub> contents a) Hydrogenation of toluene in the presence of aniline, b)**  
 242 **Isomerization/cracking of n-heptane at 360°C.**  
 243

244 The selectivity to i-heptane is shown in Figure 2. The results indicate that the selectivity increases  
 245 as the metal oxide content increases, for a given n-C<sub>7</sub> conversion. This is sign of a better  
 246 metal/acid (M/A) balance. As the metal content of the catalyst increases, the probability of an

247 intermediate i-C<sub>7</sub> olefin finding a metal site, before undergoing further isomerization and cracking  
248 increases.



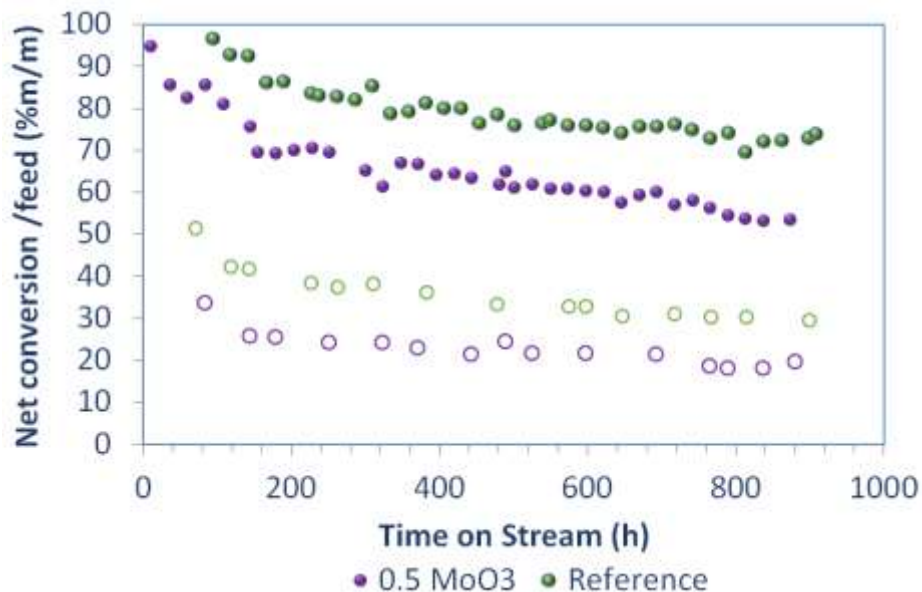
249  
250 **Figure 2. Selectivity to i-C<sub>7</sub> Vs. n-C<sub>7</sub> conversion for fresh dried catalyst samples with different MoO<sub>3</sub>**  
251 **contents.**

252  
253 Once this simple screening of the molybdenum content was accomplished, the catalyst with 50 %  
254 of the metal oxide content (designated as “0.5 MoO<sub>3</sub>”) of the reference catalyst (designated as  
255 “Reference”) was selected to evaluate its loss of activity in the pilot unit under accelerated  
256 deactivation conditions. The goal was to evaluate the impact of an important modification of the  
257 M/A ratio on catalyst activity and deactivation.

### 258 3.2 Deactivation experiments with catalysts at different metal contents

#### 259 3.2.1 Evolution of the apparent kinetic constants with time on stream

260 In the first place, the evolution of the net conversion (Equation 1) with time on stream is displayed  
261 in Figure 3 for both the first reactor and the whole system. The catalyst with the lower molybdenum  
262 content presented a lower conversion for both reactors.



263

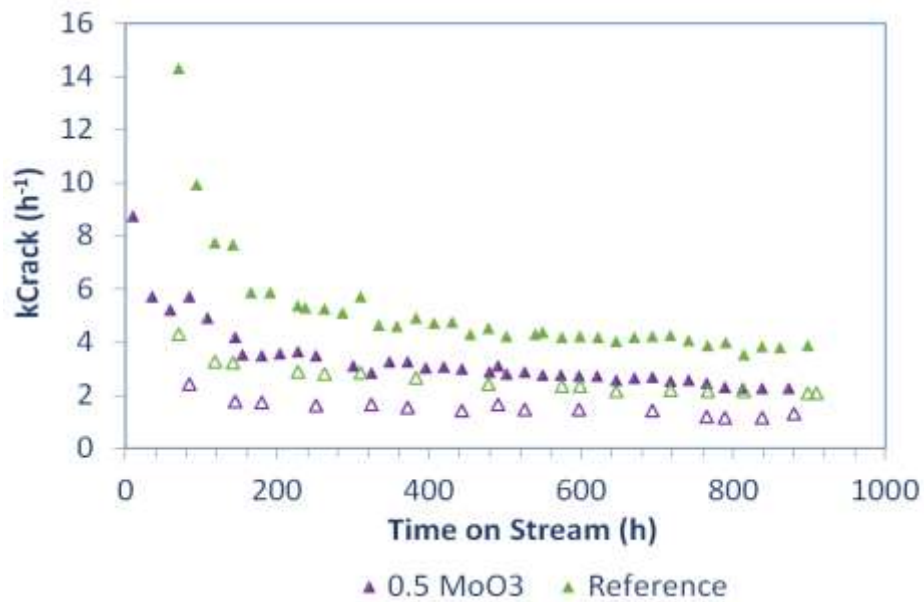
264 **Figure 3. Net conversion as a function of time on stream for catalysts with different metal**  
 265 **contents. Open symbols=First reactor effluent, Full symbols=Total effluent.**

266  
 267

268 The evolution of the apparent kinetic constants for cracking, hydrodenitrogenation (HDN), and  
 269 aromatic hydrogenation (HDA) reactions with time on stream (TOS) are shown in Figure 4, Figure  
 270 5 and Figure 6, respectively.

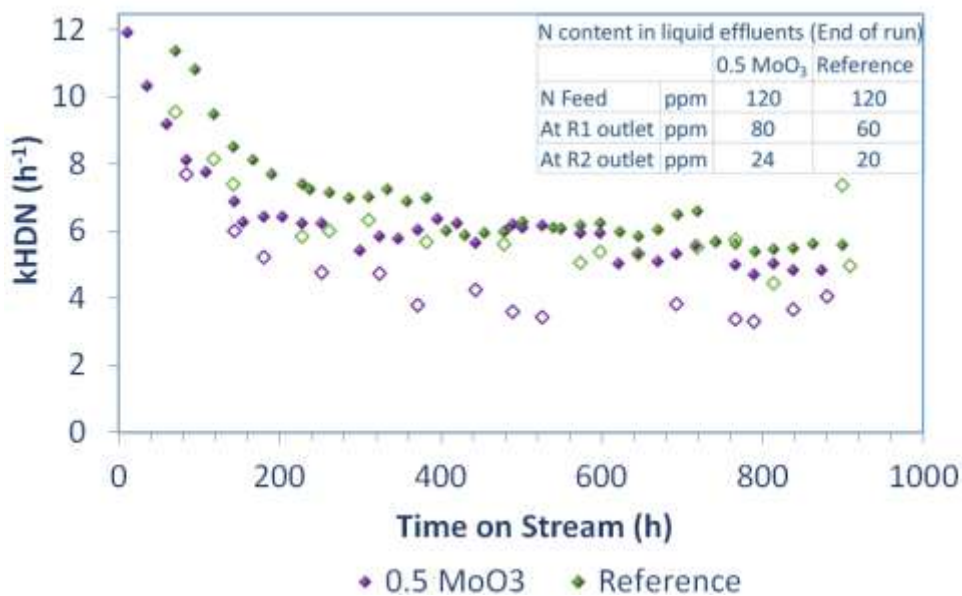
271 As was expected, the data indicate that the reduction in the amount of molybdenum (the  
 272 component responsible for the hydrogenation activity) caused a decrease in the hydrogenation  
 273 reactions of both aromatics and nitrogen compounds (Figure 5 and 6). Also, the cracking constants  
 274 decreased by about 40%. This may be explained by two factors: (i) the limitation of bifunctional  
 275 cracking by the metal function, as illustrated for n-heptane cracking in Figure 1b; (ii) the lower  
 276 HDN activity, leading to a higher organic nitrogen concentration inside the reactor in the case of  
 277 the 0.5MoO3 catalyst, which inhibits the cracking activity.

278 The kinetic rates for the mentioned reactions were lower in the first reactor than in the second one  
 279 (HDA values are not shown for the first reactor since they are negligible). This result is explained  
 280 by the organic nitrogen concentration profile along the system, that strongly inhibits both catalyst  
 281 functions.



282

283 **Figure 4. Global and first reactor kinetic constants as a function of time on stream for cracking**  
 284 **reactions for catalysts with different metal contents. Open symbols=First reactor effluent, Full**  
 285 **symbols=Total effluent.**



286

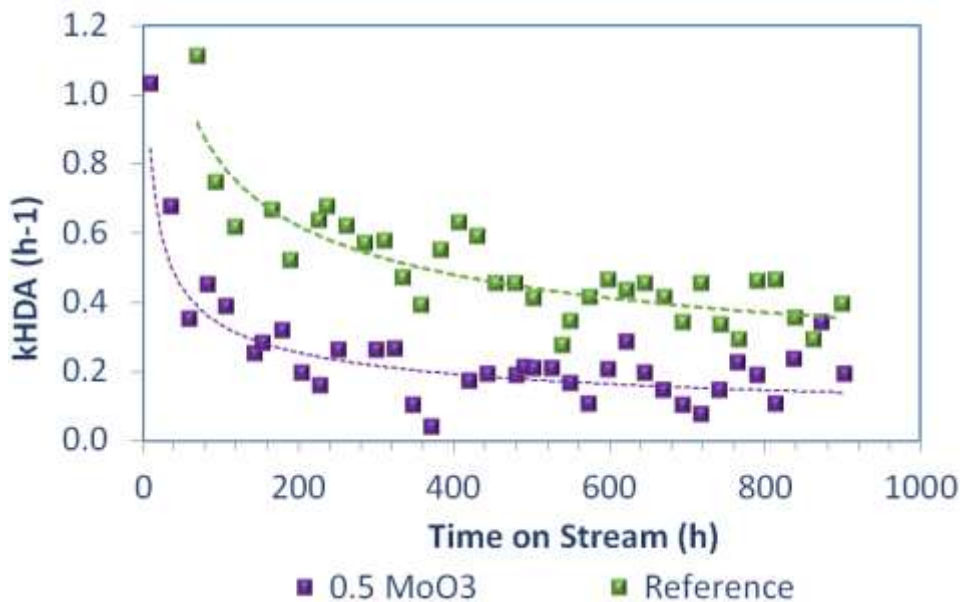
287

288

289 **Figure 5. Global and first reactor kinetic constants as a function of time on stream for HDN**  
 290 **reactions for catalysts with different metal contents. Open symbols=First reactor effluent, Full**  
 291 **symbols=Total effluent.**

292





293  
294 **Figure 6. Global reactor kinetic constants as a function of time on stream for HDA reactions for**  
295 **catalysts with different metal contents.**  
296

### 297 3.2.2 Activity loss

298 The data of the calculated rate constants as a function of time on stream were fitted to the  
299 exponential decay model (Supporting information, Figure S1 and Figure S2) presented in section  
300 2.5 (Equation 3). The coefficients for both catalysts are presented in

301 Table 3. The reference catalyst had a higher residual activity (c value) than the 0.5MoO<sub>3</sub> catalyst.

302 But the exponential decay model also indicates that the relative activity loss was faster for the  
303 catalyst with the stronger hydrogenation function and that the retained activity with respect to the  
304 initial activity was lower for this catalyst ( $c/(A+c)$ ). The inspection of the raw conversion data had  
305 suggested the opposite trend, i.e., a higher conversion loss for the 0.5MoO<sub>3</sub> catalyst (Figure 3).

306 However, as previously explained, it is more accurate to examine the evolution of the reaction rate  
307 coefficients since the interpretation of the raw conversion data can be misleading because the  
308 relationship between conversion and contact time is not linear. The higher the conversion, the  
309 greater the contact time required to increase it (higher catalyst volume). So, in our case, it is not  
310 the same to lose 25 points of conversion with the reference catalyst between 97 and 72 than to  
311 lose 31 points with the catalyst of lower molybdenum content between 85 and 54 both of them

312 during TOS from 94h to 838h. In other words, the fact that the conversion decreases from a high  
 313 conversion (97%) implies the deactivation of a larger fraction of the catalytic bed than the fraction  
 314 which is deactivated for the conversion to decrease from a value of 85%. This behavior is not  
 315 reflected in the conversion curve but in the kinetic constants, so the comparisons at different  
 316 conversion levels should be made based on these data. For the purpose of understanding, the  
 317 analysis of the evolution of apparent velocity coefficients is more appropriate.”

318

319 **Table 3. Activity loss rate coefficients ( $\alpha$ ) and residual activities (c) calculated with an exponential**  
 320 **decay model for catalysts with different metal contents.**  
 321

Catalyst	$\alpha$ (1/day)	A	c	$c/(A+c)$
0.5 MoO <sub>3</sub>	0.23	5.7	2.7	0.32
Reference	0.39	29	4.3	0.13

### 322 3.3 Spent catalysts characterization

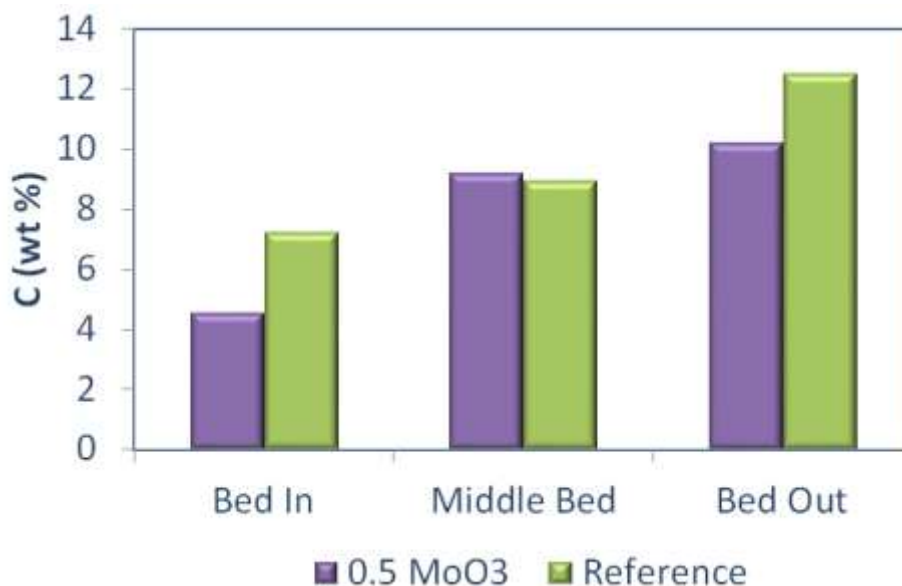
#### 323 3.3.1 Elemental analysis

324 The carbon content of the spent samples is presented in Figure 7. Contrary to what was expected,  
 325 the carbon deposition was lower for the catalyst with lower metal content. This behavior can be  
 326 attributed to the higher nitrogen concentration (lower  $k_{HDN}$  values) in the liquid phase with this  
 327 catalyst, which inhibits cracking reactions and, consequently, the polymerization reactions to form  
 328 coke. The values of the N/C ratio (Figure 8) as well as the nitrogen content in coke (Figure 9)  
 329 confirmed the latter. The nitrogen content was higher for the spent catalysts with lower  
 330 molybdenum loading. It means that the contribution to the overall coke formation from nitrogen  
 331 precursors plays a more important role for this catalyst in comparison with the reference catalyst.  
 332 For both catalysts, the carbon content along the reactor increased from the inlet to the outlet;  
 333 meanwhile, the N/C values decreased. Both facts agree with the nitrogen concentration profile,  
 334 which decreases along the length of the reactor. The preferential adsorption of the nitrogen

335 compounds on acid sites inhibits the polymerization of the dehydrogenated intermediates reducing  
336 the formation of coke deposits.

337

338

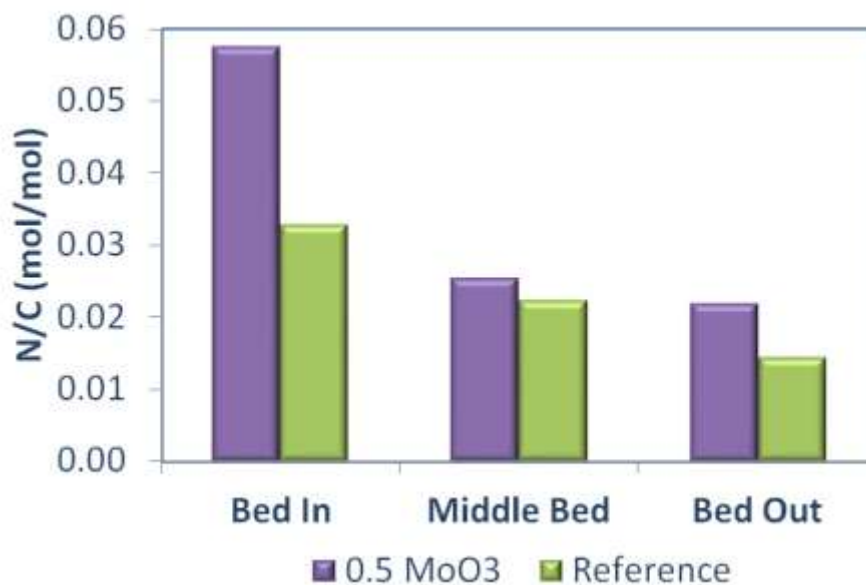


339

340 **Figure 7. Carbon contents of the spent catalysts with different metal contents. Samples taken at**  
341 **different reactor locations.**

342

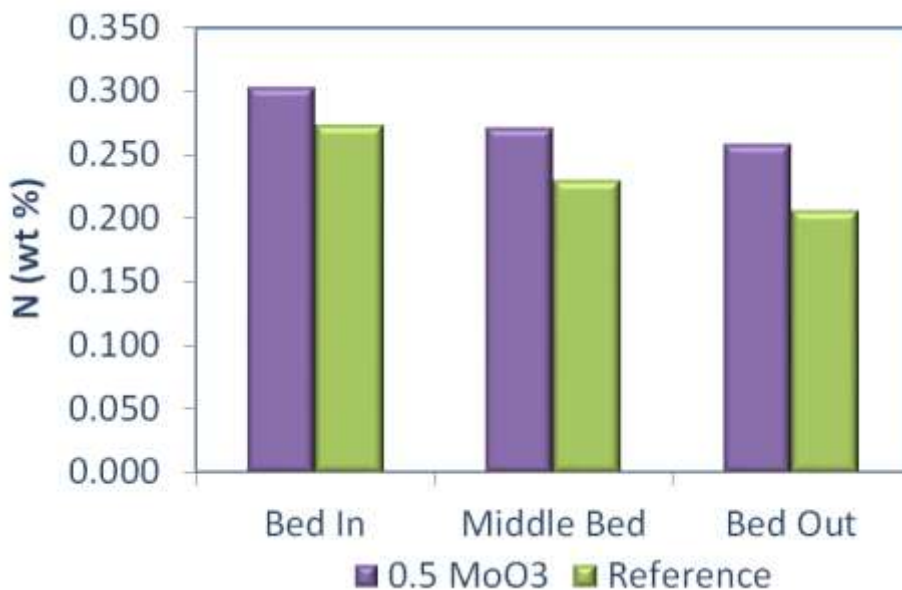
343



344

345 **Figure 8. N/C ratio of the spent catalysts with different metal contents. Samples taken at different**  
346 **reactor locations.**

347

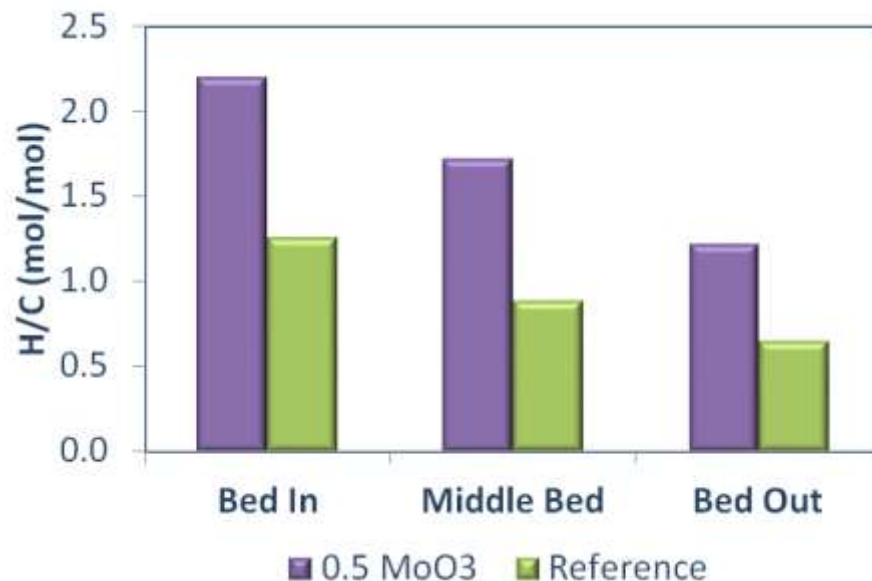


348

349 **Figure 9. Nitrogen content of the spent catalysts with different metal contents. Samples taken at**  
350 **different reactor locations.**

351

352 Results of the H/C ratio of the coke in the spent catalysts are shown in Figure 10. A lower H/C  
353 ratio (indicating a more aromatic character of the coke deposit) was observed for the carbon  
354 deposits formed on the reference catalyst than for the 0.5MoO<sub>3</sub> catalyst. It can be related to the  
355 higher cracking rate of the reference catalyst, which enhances the polymerization reactions of the  
356 coke precursors, forming more condensed structures with lower H/C ratios and with more  
357 dehydrogenation reactions. The H/C ratio (Figure 10) diminished along the catalytic bed.



358  
359 **Figure 10. Hydrogen/Carbon ratio of the spent catalysts with different metal contents. Samples**  
360 **taken at different reactor locations.**  
361  
362

363 Analysis of coke composition suggests that a proportion of the global coke originates from organic  
364 nitrogen species. However, as HDN proceeds through the reactor and nitrogen is removed, other  
365 mechanisms, such as aromatic coke formation, begin to play a more important role in catalyst  
366 deactivation. This corresponds to the results obtained in our previous work <sup>43</sup>.

### 367 3.3.2 Textural Analysis

368 Catalysts were also analyzed by nitrogen adsorption-desorption isotherms. The surface area  
369 ( $A_{\text{BET}}$ ) and pore volume (PV) with respect to the fresh catalyst are presented in Table 4. The area  
370 and volume losses for each catalyst show a direct correlation with its carbon deposition. Thus, the  
371 most significant modifications of the textural properties of the catalyst were found for the reference  
372 catalyst. A more pronounced decrease of surface and pore volume happened at the bed outlet,  
373 agreeing with the higher carbon content at this location. Table 4 also shows the ratio between the  
374 hysteresis area of each spent catalyst and the corresponding fresh catalyst, following the  
375 methodology suggested by Sámano et al. <sup>48</sup>. The higher the value, the higher the extent of catalyst

376 deactivation. The data showed a higher deactivation with the reference catalyst than with the one  
 377 containing less molybdenum. The reactor outlet values were also higher than at the reactor inlet  
 378 for the two spent catalysts, consistent with the textural and the elemental results.

379 **Table 4. Characterization of spent catalysts with different metal contents: Surface area ( $A_{\text{BET}}$ ), total**  
 380 **pore volume (PV), micropore volume ( $\mu\text{Vol}$ ) and the ratio of hysteresis area (HA) of the spent**  
 381 **catalyst relative to the fresh catalyst.**

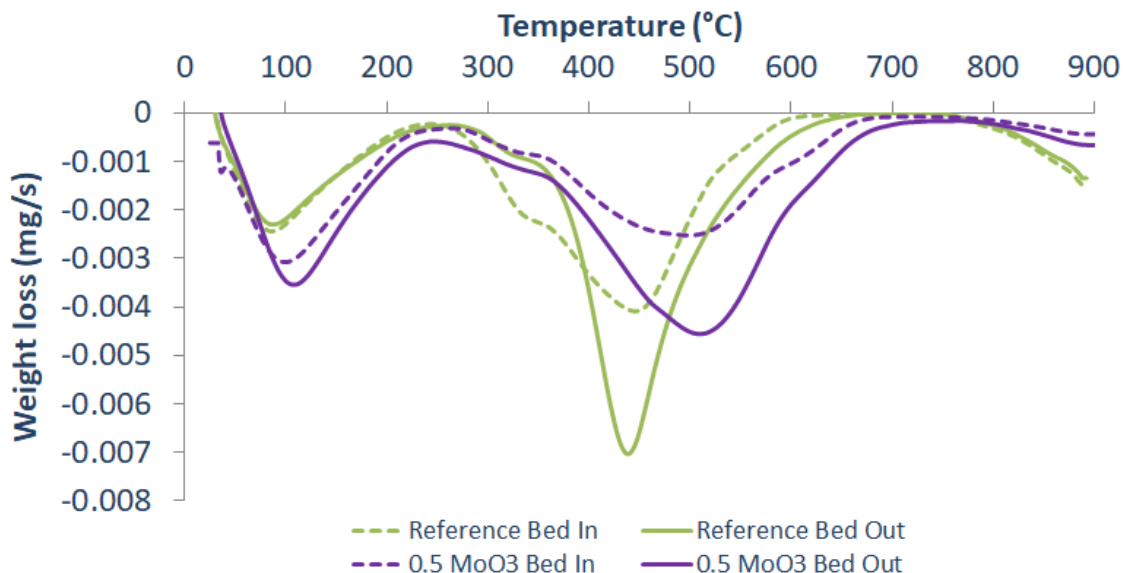
Catalyst	$A_{\text{BET}}/A_{\text{BETfresh}}$		$PV/PV_{\text{fresh}}$		$\mu\text{Vol}/\mu\text{Vol}_{\text{fresh}}$		$\frac{HA_{\text{Spent Catalyst}}}{HA_{\text{Fresh Catalyst}}}$	
	Bed Inlet (%)	Bed Outlet (%)	Bed Inlet (%)	Bed Outlet (%)	Bed Inlet (%)	Bed Outlet (%)	Bed Inlet	Bed Outlet
0.5 MoO <sub>3</sub>	82	78	85	79	68	63	1.13	1.28
Reference	82	71	78	69	61	65	1.33	1.49

382

### 383 3.3.3 Thermo-gravimetric Analysis

384 TGA analyses were done to characterize the coke deposits on the spent catalysts. The first time-  
 385 derivative of weight loss as a function of temperature is illustrated in Figure 11. The first peak,  
 386 around 100°C, corresponds to H<sub>2</sub>O desorption, the second one (280-330°C) corresponds mainly  
 387 to SO<sub>2</sub> release and the last peak is associated with the combustion of the coke deposits<sup>49,50</sup>. In

388 Table 5, the percentage of the weight loss within the range of temperature corresponding to coke  
389 deposits combustion is presented. These values agree with the carbon content from elemental  
390 analysis (see Figure 7).



391  
392 **Figure 11. TGA profiles of bed inlet and bed outlet samples from the spent catalysts with different**  
393 **metal contents. Dotted line=First reactor effluent, continuous line=Total effluent.**  
394

395 The maximum weight loss temperature is an indicator of the nature of coke; the higher this  
396 temperature, the more difficult to combust the coke is. It is often associated with a lower H/C ratio  
397 of the coke deposits. However, the coke deposits on the catalyst with less metal concentration  
398 required a higher temperature to combust (Figure 11 and

399 Table 5), although its H/C ratio is higher (Figure 10). This behavior suggests that the high-  
400 temperature peaks for this catalyst were related to the higher nitrogen content of its coke deposits  
401 (Figure 9). This is in agreement with the work of Zeuthen et al.<sup>35</sup>, who characterized some aged  
402 hydroprocessing catalysts by temperature-programmed oxidation and identified that the strongly  
403 adsorbed organic-nitrogen species are oxidized at temperatures around 500°C.

404

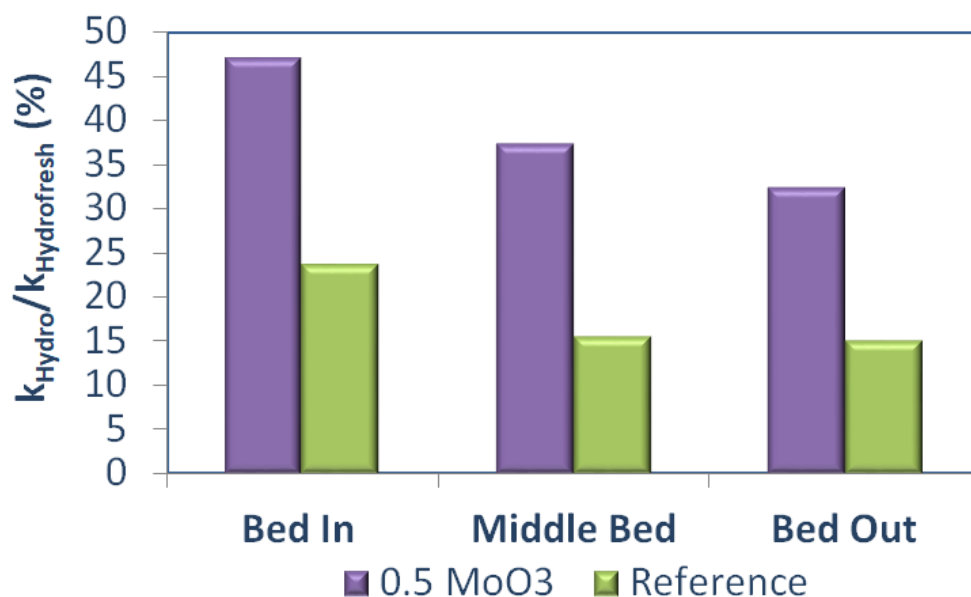


405 **Table 5. Estimation of CO<sub>2</sub> weight loss of the coke deposits and maximum peak temperature from**  
 406 **TGA profiles for spent catalysts with different metal contents.**

Catalyst	CO <sub>2</sub> weight loss (wt %)	Maximum Peak Temperature (°C)
0.5 MoO <sub>3</sub> Bed In	7.8	495
0.5 MoO <sub>3</sub> Bed Out	10.3	510
Reference Bed In	11.2	445
Reference Bed Out	16.6	440

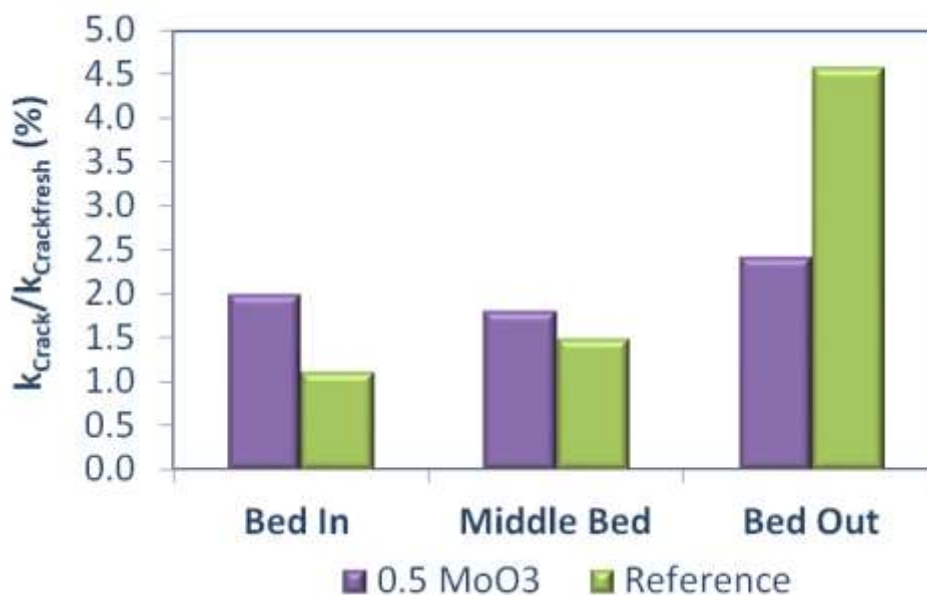
407 3.3.4 Model molecule tests

408 The residual activity of the (de)/hydrogenation and the acid functions of the spent catalysts were  
 409 characterized by toluene hydrogenation and n-heptane hydroconversion, respectively. Figure 12  
 410 illustrates the first-order rate constant of the spent catalysts relative to the corresponding fresh  
 411 catalyst ( $k_{\text{Hydro fresh}}$ ) for both studied catalysts during toluene hydrogenation ( $k_{\text{Hydro}}$ ). These values  
 412 reveal that, despite its lower initial activity, the catalysts with the lower metal content retained more  
 413 hydrogenation activity than the reference catalyst, which lost around 80% of its original activity.  
 414 The reasons for this will be discussed in the next section. The activity loss of the metal function  
 415 increased along the catalytic bed for both samples.



416  
 417 **Figure 12. Residual catalytic hydrogenation activity of the spent catalysts relative to the fresh**  
 418 **catalysts, evaluated by toluene hydrogenation. Samples taken at different reactor locations.**

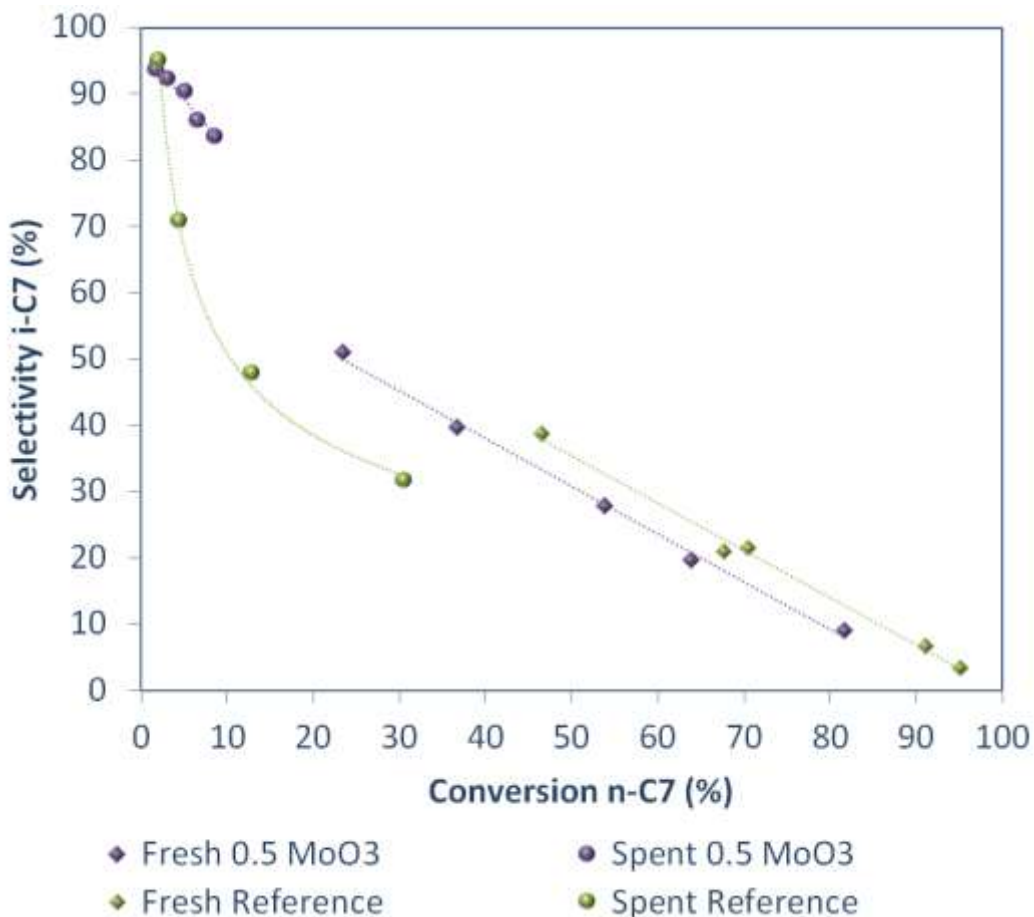
419  
420 Regarding the n-heptane cracking activity results (Figure 13), it was noticeable that it was severely  
421 deactivated in both cases. All the residual activities were below 5%. Note that, as illustrated in  
422 Figure 1b, the n-heptane cracking activity is not an exclusive measure of the acid function, but  
423 rather presents the overall bifunctional hydrocracking activity of the catalyst. For the catalyst with  
424 lower molybdenum content, the differences along the reactor were negligible. The reference  
425 catalyst had a significantly higher residual cracking activity (in absolute and in relative terms) at  
426 the bed outlet. This is attributed to the difference in nitrogen content of the carbon deposits. The  
427 reference catalyst had a significantly lower N/C ratio at the bed outlet. It seems that the nitrogen  
428 in the coke is the main cause of the decrease in residual cracking activity. We had already pointed  
429 out in our previous work<sup>51</sup> that the residual acidity of the catalyst was decorrelated from the total  
430 coke content and specifically related to nitrogen compounds.



431  
432 **Figure 13. Residual catalytic cracking activity of the spent catalysts relative to the fresh catalyst,**  
433 **evaluated by isomerization/cracking of n-heptane at 360°C. Samples taken at different reactor**  
434 **locations.**

436 The selectivity to i-heptane is presented in Figure 14. In contrast to the fresh samples, the 0.5  
437 MoO<sub>3</sub> catalyst had a higher i-heptane selectivity, meaning that the ratio between the metal and

438 acid sites (M/A) was better balanced for this catalyst. This is in line with the higher residual  
439 hydrogenation activity (Figure 12) and the lower residual cracking (Figure 13) of the 0,5 MoO<sub>3</sub>  
440 catalyst.



441

442 **Figure 14. Selectivity to i-C<sub>7</sub> Vs. conversion n-C<sub>7</sub>, obtained by n-heptane hydroconversion at**  
443 **different temperatures.**  
444

#### 445 **4 DISCUSSION**

446 Hydrocracking proceeds by bifunctional catalysis. This makes studying the deactivation very  
447 complex, because the deactivation of the overall hydrocracking activity depends on the  
448 deactivation of the metal and of the acid function as well as on the evolution of the balance  
449 between the two. We, therefore, started by evaluating the impact of metal/acid balance on the

450 activity of fresh catalysts in model reactions. As expected, on fresh catalysts, the hydrogenation  
451 activity increased (almost proportionally) with the molybdenum content (Figure 1Figure 1a). The  
452 decrease in the metal content also had a negative impact on the activity of the cracking function  
453 (Figure 1b). This result agrees with other authors <sup>14</sup>, who established that at low metal/acid (M/A)  
454 ratios, there is a limitation of the bifunctional mechanism by the (de)-hydrogenation steps. This  
455 means that the metal sites are not sufficiently abundant to provide olefins for all the acid sites, so  
456 the maximum activity of the cracking function cannot be exploited. A decrease in the overall activity  
457 of the catalyst is then observed. The fact that the decrease is more pronounced than in some other  
458 recent studies on sulfide hydrocracking catalysts <sup>19,23,24</sup> indicates that our catalysts covered a  
459 range of lower M/A ratios than the works cited above.

460 During the pilot plant deactivation experiments, the following differences in the behavior of the 0.5  
461 MoO<sub>3</sub> catalyst with respect to the reference catalyst were observed in terms of reactivity:

- 462 • A lower cracking activity, but also a slower (relative) deactivation.
- 463 • A lower hydrodenitrogenation (HDN) and aromatics hydrogenation (HDA) activity.

464 In terms of characterization of the spent catalyst, it was observed that the 0.5 MoO<sub>3</sub> catalyst:

- 465 • Had a lower amount of coke, associated with a lower loss of surface area and pore volume.
- 466 • Had a higher nitrogen content (and, thus, a higher N/C ratio).
- 467 • Retained a higher percentage of its initial hydrogenation activity.
- 468 • Retained a higher percentage of its initial cracking activity at the bed inlet, but a lower  
469 percentage at the bed outlet.

470 In the following discussion, we will try to rationalize these trends. In our earlier work, we had seen  
471 that the deactivation process is largely governed by the presence of organic nitrogen species,  
472 which in turn determines the metal/acid balance <sup>43</sup>. The lower the HDN activity, the higher is the  
473 nitrogen compounds' concentration along the catalytic bed. This higher concentration has a strong  
474 repercussion on the catalytic performance since nitrogen derivatives are known to be inhibitors of

475 the metal sites<sup>43,52-55</sup> and especially of the acid sites<sup>23,43</sup>, where they are strongly adsorbed<sup>56-59</sup>.  
476 The inhibition of the acid and metal sites has two antagonistic effects with respect to coke  
477 formation. On the one hand, the adsorbed nitrogen compounds may eventually be converted to  
478 coke, permanently deactivating the acid sites. Moreover, the inhibition of the hydrogenation activity  
479 of the metal sites leads to an increase in aromatics concentration along the reactor. If there are  
480 sufficiently available acid sites, the aromatics undergo addition, dehydrogenation and hydrogen  
481 transfer reactions to grow into large polyaromatic molecules, i.e., coke precursors<sup>3,60</sup>. On the other  
482 hand, this coke deposition from aromatics is slowed down by the progressive inhibition of acid  
483 sites by nitrogen compounds<sup>61</sup>. The data shown in this paper demonstrate that the latter effect  
484 dominates over the former ones. Despite its lower HDN and HDA activity, i.e., despite of a higher  
485 concentration of coke precursors, the 0.5 MoO<sub>3</sub> catalyst generated less coke. This must be related  
486 to the lower availability of acid sites (i.e., a stronger inhibition by nitrogen compounds with respect  
487 to the reference catalyst).

488 The spent catalyst samples with the lower molybdenum concentration presented higher nitrogen  
489 contents and higher N/C ratios than the spent reference catalyst, especially at the bed inlet (Figure  
490 8 and Figure 9), meaning that the contribution of nitrogen compounds to the overall coke formation  
491 was higher for this catalyst. This result is linked to the more nitrogen-rich atmosphere in the reactor  
492 when the 0.5 MoO<sub>3</sub> catalyst was used. The reference catalyst exhibited a higher amount of coke  
493 with less nitrogen, i.e., a more significant contribution to the global coke formation came from  
494 aromatic compounds (whose condensation reactions are catalyzed by the acid sites). This can  
495 also explain the lower H/C ratio (Figure 10) of these samples.

496 Regarding the residual activities of the spent samples, it was observed that the loss of  
497 hydrogenating activity was more pronounced for the reference catalyst (Figure 12). Since no  
498 meaningful differences were observed in sintering or depromotion between the spent samples  
499 (Supporting information table S1, TEM analysis), this behavior was attributed to a higher coke

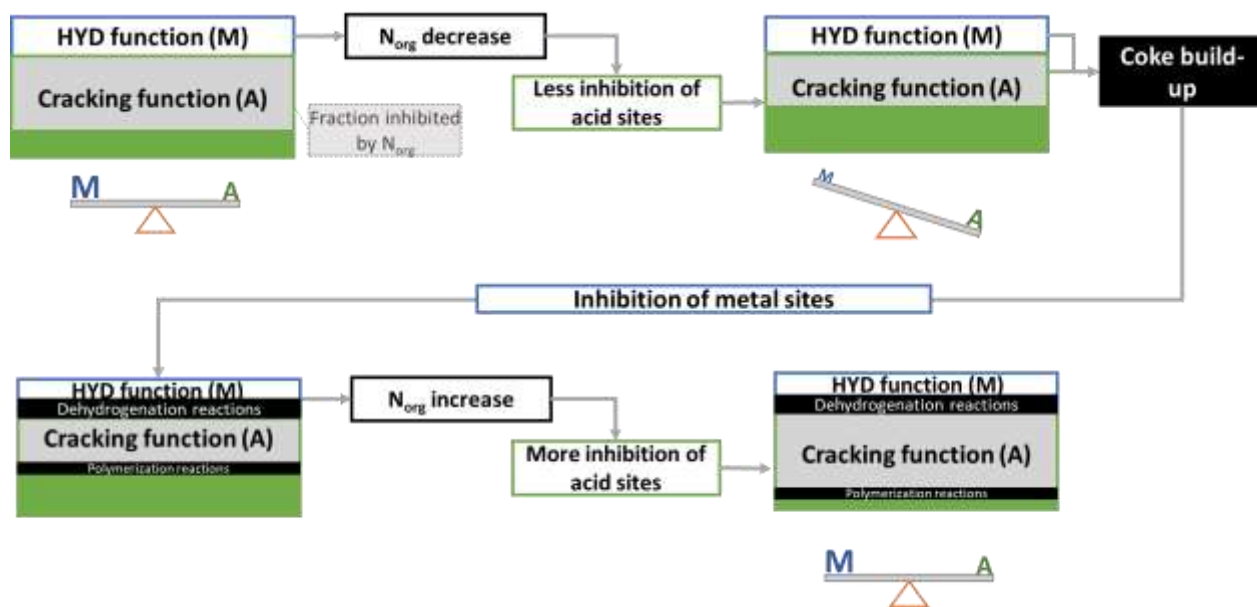
500 build-up with the reference catalyst. In reference <sup>51</sup>, we had already observed a strong correlation  
501 between the amount of coke formation and the loss of hydrogenation activity. The coke deposition  
502 is determined by the metal/acid (M/A) balance. Figure 14 shows that the M/A balance was less  
503 favorable for the spent reference catalyst (less metal sites vs. acid sites). This explains the higher  
504 coke formation on this catalyst, which in turn leads to a strong deactivation of the metal function  
505 (this feedback loop will be discussed later in the text).

506 The residual n-heptane hydrocracking activity was very low for both samples. The 0.5 MoO<sub>3</sub>  
507 catalyst had a lower cracking activity than the reference catalysts at the bed outlet (Figure 913).  
508 This is attributed to the higher nitrogen content of the coke on the 0.5 MoO<sub>3</sub> samples (Figure 9  
509 because the nitrogen species are strongly adsorbed on the acid sites, deactivating them. As  
510 mentioned before, this catalyst exhibited a lower carbon deposition, which can be attributed to a  
511 more favorable M/A balance.

512 When making the link between the results of the model molecule tests and the VGO deactivation  
513 experiments, we see that the 0.5 MoO<sub>3</sub> catalyst generated less coke and lost less VGO  
514 hydrocracking activity (in relative terms, see Figure 4 and Table 3). The latter observation is  
515 seemingly in contradiction with Figure 13, which shows that it lost, on average, a higher  
516 percentage of its residual n-heptane cracking activity. In order to resolve this dilemma, we have  
517 to make the hypothesis that the M/A balance does not have the same impact in n-heptane cracking  
518 and in the VGO deactivation test. In n-heptane cracking, the fresh reference catalyst was fairly  
519 well balanced, but became extremely badly balanced after deactivation (Figure 14). We  
520 hypothesize that this did not strongly impact its n-heptane hydrocracking activity, but had strong  
521 repercussions on its VGO hydrocracking activity. In other words, the stronger deactivation of the  
522 reference catalyst would, after all, be mainly related to the stronger deactivation of its  
523 hydrogenation function and not of its acid function. We admit, however, that this is just a  
524 hypothesis for moment, which should be confirmed by complementary experimentation.

525 Let us finally come back to the above-mentioned negative feedback loop of deactivation. If we  
526 have a hydrocracking catalyst with a strong hydrogenation function (our reference catalyst), it will  
527 lead to a quick drop of the organic nitrogen profile in the reactor. This leads in turn to an imbalance  
528 of the M/A ratio. This imbalance is the main cause of coke formation. Unsaturated coke precursors  
529 produced on the acid sites undergo polymerization reactions before being hydrogenated and  
530 successive dehydrogenation reactions occurred on metal sites leading to partially hydrogenated  
531 intermediates that combine to form coke. The formed coke deactivates both functions, but in a  
532 more significant way the hydrogenation function <sup>51</sup>, since the cracking function is mainly affected  
533 by the nitrogen compounds. This phenomenon leads to a negative feedback loop, which is  
534 illustrated in Figure 15. When the hydrogenating function is deactivated by coke build up, the  
535 nitrogen concentration increases progressively. Therefore, more acid sites are neutralized so that  
536 the M/A balance tends to recover, and coke formation slows down. In other words, the coke  
537 formation provides negative feedback on deactivation; thus, the deactivation rate slows down over  
538 time.

539



540

541 **Figure 15. Schematic representation of the deactivation cycle of the acid and hydrogen functions**  
 542 **of a bifunctional catalyst in a nitrogen-rich atmosphere. The hydrogenation function is represented**  
 543 **by a blue rectangle, the cracking function by a green rectangle, coke on the metal function in**  
 544 **black, the inhibited fraction of the cracking function in grey.**  
 545

546 In general, our data show that the modification of the hydrogenation function of VGO  
 547 hydrocracking catalysts has two main consequences: a reduction of the HDN activity and a  
 548 reduction of the cracking activity. The balance between these two phenomena leads to  
 549 unexpected behavior with respect to deactivation in organic nitrogen-poor atmospheres. Current  
 550 literature states that a reduction in the hydrogenating function for samples with the same acid  
 551 function, leads to more coke formation on the catalyst, which provokes rapid deactivation<sup>13,14,17</sup>.  
 552 However, this study showed that this does not hold true for nitrogen-rich reaction systems. In this  
 553 case, the decrease in the hydrogenating function causes an indirect decrease in the acid function  
 554 of the catalyst, due to a stronger inhibition by nitrogen compounds. This provokes a modification  
 555 on the M/A ratio, so the spent catalyst containing a lower Mo content actually shows a better  
 556 balance. Consequently, less coke generation was observed, with a lower aromatic character, but  
 557 with higher nitrogen content. Therefore, the deactivation was lower for the catalyst with a weaker  
 558 hydrogenating function.



559 We have seen that many of the deactivation phenomena that we observed are dictated by the  
560 behavior of the organic nitrogen compounds. It would be desirable to carry out a similar study with  
561 nitrogen-poor feeds, where inhibition effects play a smaller role. However, in practice, this is not  
562 easily reconciled with the ambition of an accelerated deactivation protocol: the high concentration  
563 of organic nitrogen allows us to operate at high temperatures, which enhances deactivation.

## 564 **5 CONCLUSIONS**

- 565 • The balance between the metal and the acid functions determines the rate-limiting step of the  
566 bifunctional reaction mechanism. In case of a significant reduction in the metal content, the  
567 initial (de)/hydrogenation reactions may become the rate limiting step of the mechanism.  
568 Therefore, the global catalyst activity decreases.
- 569 • In hydrocracking of feedstocks with high nitrogen content, the decrease of the metal content  
570 of a bifunctional catalyst causes a substantial increase in the concentration of nitrogen  
571 compounds in the catalytic bed. This increase determines the performance of the catalyst by  
572 significantly reducing the available acid sites. Thus, there is a modification in the M/A ratio  
573 favoring a better balance of the spent catalyst resulting in a lower coke deposition and  
574 therefore, a lower deactivation rate.
- 575 • The interplay between HDN and cracking in VGO hydroprocessing leads to perverse effects,  
576 i.e., an improvement of the M/A balance when reducing the metal content, via the mechanism  
577 explained above. The direct effect of the reduction of the metal content and its indirect  
578 consequence, which is an increase in the acid sites inhibition by nitrogen, have an  
579 antagonistic influence on the deactivation behavior. The balance between both effects is  
580 expected to subtly depend on the properties of both the feed and the catalyst. This study  
581 provides a methodology for studying this complex system and a framework for interpreting  
582 the results, but one should be careful in generalizing the trends observed in this e, because

583 they may depend on the system under consideration. Therefore, for systems with lower  
584 nitrogen contents, a specific study should be carried out.

585 • Our data also explains why deactivation slows down with time via an autoregulation  
586 phenomenon. A strong metal function in the fresh catalyst leads to a fast initial coke build up  
587 (by creating a M/A imbalance via the mechanism explained above). The coke builds up  
588 specifically deactivates the metal function, thereby restoring the M/A balance and coke  
589 formation slows down.

590

591 **Supporting Information:** Available as supporting information are the fits by the exponential decay  
592 model and the TEM analyses of the catalysts.

593

594 6 References

- 595 (1) Toulhoat, H.; Raybaud, P., Eds. *Catalysis by transition metal sulphides: From molecular theory*  
596 *to industrial application*; IFP énergies nouvelles publications; Éd. Technip, 2013.
- 597 (2) Scherzer, J.; Gruia, A. J. *Hydrocracking science and technology*; Chemical industries, Vol. 66;  
598 Marcel Dekker, 1996.
- 599 (3) Speight, J. G. *The refinery of the future*, 1st edition; Elsevier; Gulf Professional Publishing,  
600 2011.
- 601 (4) Ward, J. W. Hydrocracking processes and catalysts. *Fuel Processing Technology* 1993, 35  
602 (1-2), 55–85. DOI: 10.1016/0378-3820(93)90085-I.
- 603 (5) Leprince, P. Petroleum refining. *Petroleum refining* 2001.
- 604 (6) *Advances in Catalysis*; Elsevier Science, 2016.
- 605 (7) Vogt, E. T.; Whiting, G. T.; Dutta Chowdhury, A.; Weckhuysen, B. M. Zeolites and Zeotypes  
606 for Oil and Gas Conversion. In; *Advances in Catalysis*; Elsevier, 2015; pp 143–314. DOI:  
607 10.1016/bs.acat.2015.10.001.
- 608 (8) Weitkamp, J. Catalytic Hydrocracking—Mechanisms and Versatility of the Process.  
609 *ChemCatChem* 2012, 4 (3), 292–306. DOI: 10.1002/cctc.201100315.
- 610 (9) Batalha, N.; Pinard, L.; Bouchy, C.; Guillon, E.; Guisnet, M. n-Hexadecane hydroisomerization  
611 over Pt-HBEA catalysts. Quantification and effect of the intimacy between metal and protonic sites.  
612 *Journal of Catalysis* 2013, 307, 122–131. DOI: 10.1016/j.jcat.2013.07.014.
- 613 (10) Coonradt, H. L.; Garwood, W. E. Mechanism of Hydrocracking. Reactions of Paraffins and  
614 Olefins. *Ind. Eng. Chem. Proc. Des. Dev.* 1964, 3 (1), 38–45. DOI: 10.1021/i260009a010.
- 615 (11) Weisz, P. B. Polyfunctional Heterogeneous Catalysis. In ; *Advances in Catalysis*; Elsevier,  
616 1962; pp 137–190. DOI: 10.1016/S0360-0564(08)60287-4.
- 617 (12) Weitkamp, J. Isomerization of long-chain n-alkanes on a Pt/CaY zeolite catalyst. *Ind. Eng.*  
618 *Chem. Prod. Res. Dev.* 1982, 21 (4), 550–558. DOI: 10.1021/i300008a008.

619 (13) Guisnet, M.; Alvarez, F.; Giannetto, G.; Perot, G. Hydroisomerization and hydrocracking of  
620 n-heptane on Pth zeolites. Effect of the porosity and of the distribution of metallic and acid sites.  
621 *Catalysis Today* 1987, 1 (4), 415–433. DOI: 10.1016/0920-5861(87)80007-X.

622 (14) Giannetto, G. E.; Perot, G. R.; Guisnet, M. R. Hydroisomerization and hydrocracking of n-  
623 alkanes. 1. Ideal hydroisomerization PtHY catalysts. *Ind. Eng. Chem. Prod. Res. Dev.* 1986, 25  
624 (3), 481–490. DOI: 10.1021/i300023a021.

625 (15) Francis, J.; Guillon, E.; Bats, N.; Pichon, C.; Corma, A.; Simon, L. J. Design of improved  
626 hydrocracking catalysts by increasing the proximity between acid and metallic sites. *Applied*  
627 *Catalysis A: General* 2011, 409-410, 140–147. DOI: 10.1016/j.apcata.2011.09.040.

628 (16) Derouane, E. G.; Lemos, F.; Naccache, C.; Ribeiro, F. R. *Zeolite Microporous Solids:*  
629 *Synthesis, Structure, and Reactivity*; Springer Netherlands, 1992. DOI: 10.1007/978-94-011-  
630 2604-5.

631 (17) Alvarez, F.; Ribeiro, F. R.; Perot, G.; Thomazeau, C.; Guisnet, M. Hydroisomerization and  
632 Hydrocracking of Alkanes. *Journal of Catalysis* 1996, 162 (2), 179–189. DOI:  
633 10.1006/jcat.1996.0275.

634 (18) Guisnet, M. “Ideal” bifunctional catalysis over Pt-acid zeolites. *Catalysis Today* 2013, 218-  
635 219, 123–134. DOI: 10.1016/j.cattod.2013.04.028.

636 (19) Pirngruber, G. D.; Maury, S.; Daudin, A.; Alspektor, P. Y.; Bouchy, C.; Guillon, E. Balance  
637 between (De)hydrogenation and Acid Sites: Comparison between Sulfide-Based and Pt-Based  
638 Bifunctional Hydrocracking Catalysts. *Ind. Eng. Chem. Res.* 2020, 59 (28), 12686–12695. DOI:  
639 10.1021/acs.iecr.0c01680.

640 (20) Regali, F.; Liotta, L. F.; Venezia, A. M.; Boutonnet, M.; Järås, S. Hydroconversion of n-  
641 hexadecane on Pt/silica-alumina catalysts: Effect of metal loading and support acidity on  
642 bifunctional and hydrogenolytic activity. *Applied Catalysis A: General* 2014, 469, 328–339. DOI:  
643 10.1016/j.apcata.2013.09.048.

644 (21) Degnan, T. F.; Kennedy, C. R. Impact of catalyst acid/metal balance in hydroisomerization  
645 of normal paraffins. *AIChE J.* 1993, 39 (4), 607–614. DOI: 10.1002/aic.690390409.

646 (22) Denayer, J. F.; Baron, G. V.; Vanbutsele, G.; Jacobs, P. A.; Martens, J. A. Evidence for  
647 Alkylcarbenium Ion Reaction Intermediates from Intrinsic Reaction Kinetics of C6–C9n-Alkane  
648 Hydroisomerization and Hydrocracking on Pt/H–Y and Pt/USY Zeolites. *Journal of Catalysis* 2000,  
649 190 (2), 469–473. DOI: 10.1006/jcat.1999.2756.

650 (23) Mendes, P. S.; Silva, J. M.; Ribeiro, M. F.; Bouchy, C.; Daudin, A. Quantification of the  
651 available acid sites in the hydrocracking of nitrogen-containing feedstocks over USY shaped  
652 NiMo-catalysts. *Journal of Industrial and Engineering Chemistry* 2019, 71, 167–176. DOI:  
653 10.1016/j.jiec.2018.11.019.

654 (24) Mendes, P. S. F.; Silva, J. M.; Ribeiro, M. F.; Daudin, A.; Bouchy, C. Bridging the gap  
655 between academic and industrial hydrocracking: On catalyst and operating conditions' effects.  
656 *Catal. Sci. Technol.* 2020, 10 (15), 5136–5148. DOI: 10.1039/D0CY00568A.

657 (25) Bukhtiyarova, M. V.; Toktarev, A. V.; Kazakov, M. O.; Kodenev, E. G.; Pereyma, V. Y.;  
658 Gabrienko, A. A.; Bukhtiyarov, A. V.; Echevsky, G. V. Effect of sulfosalicylic acid treatment on the  
659 properties of Beta zeolite and performance of NiW/Beta-based catalysts in hexadecane  
660 hydrocracking. *Applied Catalysis A: General* 2020, 598, 117573. DOI:  
661 10.1016/j.apcata.2020.117573.

662 (26) Danilova, I. G.; Dik, P. P.; Sorokina, T. P.; Gabrienko, A. A.; Kazakov, M. O.; Paukshtis, E.  
663 A.; Doronin, V. P.; Klimov, O. V.; Noskov, A. S. Effect of rare earths on acidity of high-silica  
664 ultrastable REY zeolites and catalytic performance of NiMo/REY+Al<sub>2</sub>O<sub>3</sub> catalysts in vacuum gas  
665 oil hydrocracking. *Microporous and Mesoporous Materials* 2022, 329, 111547. DOI:  
666 10.1016/j.micromeso.2021.111547.

667 (27) Furimsky, E. Deactivation of hydroprocessing catalysts. *Catalysis Today* 1999, 52 (4), 381–  
668 495. DOI: 10.1016/S0920-5861(99)00096-6.

669 (28) Gualda, G.; Toulhoat, H. Etude de la desactivation des catalyseurs d'hydrotraitement par  
670 cokage. Synthèse bibliographique. *Rev. Inst. Fr. Pét.* 1988, 43 (4), 567–594. DOI:  
671 10.2516/ogst:1988036.

672 (29) Furimsky, E. *Catalysts for upgrading heavy petroleum feeds*; Studies in surface science and  
673 catalysis; Elsevier, 2007.

674 (30) Argyle, M.; Bartholomew, C. Heterogeneous Catalyst Deactivation and Regeneration: A  
675 Review. *Catalysts* 2015, 5 (1), 145–269. DOI: 10.3390/catal5010145.

676 (31) Dong, D.; Jeong, S.; Massoth, F. E. Effect of nitrogen compounds on deactivation of  
677 hydrotreating catalysts by coke. *Catalysis Today* 1997, 37 (3), 267–275. DOI: 10.1016/S0920-  
678 5861(97)00022-9.

679 (32) Absi-Halabi, M.; Stanislaus, A.; Trimm, D. L. Coke formation on catalysts during the  
680 hydroprocessing of heavy oils. *Applied Catalysis* 1991, 72 (2), 193–215. DOI: 10.1016/0166-  
681 9834(91)85053-X.

682 (33) Park, Y. C.; Rhee, H.-K. The role of nickel in pyridine hydrodenitrogenation over NiMo/Al<sub>2</sub>O<sub>3</sub>.  
683 *Korean J. Chem. Eng.* 1998, 15 (4), 411–416. DOI: 10.1007/BF02697131.

684 (34) Sau, M.; Basak, K.; Manna, U.; Santra, M.; Verma, R. P. Effects of organic nitrogen  
685 compounds on hydrotreating and hydrocracking reactions. *Catalysis Today* 2005, 109 (1-4), 112–  
686 119. DOI: 10.1016/j.cattod.2005.08.007.

687 (35) Zeuthen, P.; Blom, P.; Massoth, F. E. Characterization of nitrogen on aged hydroprocessing  
688 catalysts by temperature-programmed oxidation. *Applied Catalysis* 1991, 78 (2), 265–276. DOI:  
689 10.1016/0166-9834(91)80111-9.

690 (36) Zeuthen, P.; Blom, P.; Muegge, B.; Massoth, F. E. Temperature-programmed sulfidation and  
691 oxidation of Ni-Mo/alumina catalysts and reaction with ammonia. *Applied Catalysis* 1991, 68 (1),  
692 117–130. DOI: 10.1016/S0166-9834(00)84097-X.

693 (37) Zeuthen, P.; Cooper, B. H.; Clark, F. T.; Arters, D. Characterization and Deactivation Studies  
694 of Spent Resid Catalyst from Ebullating Bed Service. *Ind. Eng. Chem. Res.* 1995, 34 (3), 755–  
695 762. DOI: 10.1021/ie00042a007.

696 (38) Trimm, D. L. Catalyst design for reduced coking (review). *Applied Catalysis* 1983, 5 (3), 263–  
697 290. DOI: 10.1016/0166-9834(83)80156-0.

698 (39) Barbier, J.; Corro, G.; Zhang, Y.; Bournville, J. P.; Franck, J. P. Coke formation on bimetallic  
699 platinum/rhenium and platinum/iridium catalysts. *Applied Catalysis* 1985, 16 (2), 169–177. DOI:  
700 10.1016/S0166-9834(00)84470-X.

701 (40) Barbier, J. Deactivation of reforming catalysts by coking - a review. *Applied Catalysis* 1986,  
702 23 (2), 225–243. DOI: 10.1016/S0166-9834(00)81294-4.

703 (41) C.A. Querini, N.S. Figoli and J.M. Parera. Hydrocarbons reforming on Pt-Re-/Al<sub>2</sub>O<sub>3</sub>-Cl coked  
704 in a commercial reactor. *Applied Catalysis*, 1989, 249–262.

705 (42) Augustine, S. The effect of Re, S, and Cl on the deactivation of Pt/\$\gamma\$-Al<sub>2</sub>O<sub>3</sub> reforming  
706 catalysts. *Journal of Catalysis* 1989, 115 (1), 217–232. DOI: 10.1016/0021-9517(89)90020-1.

707 (43) Vivas-Báez, J. C.; Servia, A.; Pirngruber, G. D.; Dubreuil, A.-C.; Pérez-Martínez, D. J.  
708 Insights in the phenomena involved in deactivation of industrial hydrocracking catalysts through  
709 an accelerated deactivation protocol. *Fuel* 2021, 303, 120681. DOI: 10.1016/j.fuel.2021.120681.

710 (44) M. Rashidzadeh, A. Ahmad, S. Sadighi. Studying of Catalyst Deactivation in a Commercial  
711 Hydrocracking Process (ISOMAX). *Journal of Petroleum Science and Technology* 2011, 1 (1),  
712 46–54.

713 (45) Ancheyta, J.; Angeles, M. J.; Macías, M. J.; Marroquín, G.; Morales, R. Changes in Apparent  
714 Reaction Order and Activation Energy in the Hydrodesulfurization of Real Feedstocks. *Energy*  
715 *Fuels* 2002, 16 (1), 189–193. DOI: 10.1021/ef0101917.

716 (46) Lauritsen, J. V.; Bollinger, M. V.; Lægsgaard, E.; Jacobsen, K. W.; Nørskov, J. K.; Clausen,  
717 B. S.; Topsøe, H.; Besenbacher, F. Atomic-scale insight into structure and morphology changes

718 of MoS<sub>2</sub> nanoclusters in hydrotreating catalysts. *Journal of Catalysis* 2004, 221 (2), 510–522.  
719 DOI: 10.1016/j.jcat.2003.09.015.

720 (47) Arancon, R.; Saab, M.; Morvan, A.; Bonduelle-Skrzypczak, A.; Taleb, A.-L.; Gay, A.-S.;  
721 Legens, C.; Ersen, O.; Searles, K.; Mougel, V.; Fedorov, A.; Copéret, C.; Raybaud, P. Combined  
722 Experimental and Theoretical Molecular Approach of the Catalytically Active Hydrotreating MoS<sub>2</sub>  
723 Phases Promoted by 3d Transition Metals. *J. Phys. Chem. C* 2019, 123 (40), 24659–24669. DOI:  
724 10.1021/acs.jpcc.9b08437.

725 (48) Sámano, V.; Rana, M. S.; Ancheyta, J. An easy approach based on textural properties to  
726 evaluate catalyst deactivation during heavy oil hydrotreating. *Catalysis Communications* 2020,  
727 133, 105823. DOI: 10.1016/j.catcom.2019.105823.

728 (49) M.A. Callejas, M.T. Martínez, T. Blasco, E. Sastre. Coke characterisation in aged residue  
729 hydrotreating catalysts by solid-state <sup>13</sup>C-NMR spectroscopy and temperature-programmed  
730 oxidation. *Applied Catalysis A: General* 2001 (218), 181–188.

731 (50) C.A. Querini, N.S. Figoli, J.M. Parera. Hydrocarbons reforming on Pt-Re-S/Al<sub>2</sub>O<sub>3</sub>-Cl coked  
732 in a commercial reactor. *Applied Catalysis* 1989 (52).

733 (51) Vivas-Báez, J. C.; Pirngruber, G. D.; Servia, A.; Dubreuil, A.-C.; Pérez-Martínez, D. J. Impact  
734 of Feedstock Properties on the Deactivation of a Vacuum Gas Oil Hydrocracking Catalyst. *Energy*  
735 *Fuels* 2021. DOI: 10.1021/acs.energyfuels.1c00965.

736 (52) Kraus, H.; Prins, R. The Effect of Phosphorus on Oxidic NiMo(CoMo)/γ-Al<sub>2</sub>O<sub>3</sub> Catalysts: A  
737 Solid State NMR Investigation. *Journal of Catalysis* 1997, 170 (1), 20–28. DOI:  
738 10.1006/jcat.1997.1728.

739 (53) Hrabar, A.; Hein, J.; Gutiérrez, O. Y.; Lercher, J. A. Selective poisoning of the direct  
740 denitrogenation route in o-propylaniline HDN by DBT on Mo and NiMo/γ-Al<sub>2</sub>O<sub>3</sub> sulfide catalysts.  
741 *Journal of Catalysis* 2011, 281 (2), 325–338. DOI: 10.1016/j.jcat.2011.05.017.

742 (54) *IEEE Global Telecommunications Conference and Exhibition. Communications for the*  
743 *Information Age*; IEEE, 1988.



744 (55) Ho, T. Poisoning effect of ethylcarbazole on hydrodesulfurization of 4,6-  
745 diethyldibenzothiophene. *Journal of Catalysis* 2004, 222 (2), 450–460. DOI:  
746 10.1016/j.jcat.2003.12.010.

747 (56) Celis-Cornejo, C. M.; Pérez-Martínez, D. J.; Orrego-Ruiz, J. A.; Baldovino-Medrano, V. G.  
748 Identification of Refractory Weakly Basic Nitrogen Compounds in a Deeply Hydrotreated Vacuum  
749 Gas Oil and Assessment of the Effect of Some Representative Species over the Performance of  
750 a Ni–MoS<sub>2</sub>/Y-Zeolite–Alumina Catalyst in Phenanthrene Hydrocracking. *Energy Fuels* 2018, 32  
751 (8), 8715–8726. DOI: 10.1021/acs.energyfuels.8b02045.

752 (57) Khalil, I.; Celis-Cornejo, C. M.; Thomas, K.; Bazin, P.; Travert, A.; Pérez-Martínez, D. J.;  
753 Baldovino-Medrano, V. G.; Paul, J. F.; Maugé, F. In Situ IR-ATR Study of the Interaction of  
754 Nitrogen Heteroaromatic Compounds with HY Zeolites: Experimental and Theoretical  
755 Approaches. *ChemCatChem* 2020, 12 (4), 1095–1108. DOI: 10.1002/cctc.201901560.

756 (58) C.H. Bartholomew. Mechanisms of catalyst deactivation. *Applied Catalysis A: General*, 2001,  
757 17–60.

758 (59) Vogelaar, B. M.; Eijsbouts, S.; Bergwerff, J. A.; Heiszwolf, J. J. Hydroprocessing catalyst  
759 deactivation in commercial practice. *Catalysis Today* 2010, 154 (3-4), 256–263. DOI:  
760 10.1016/j.cattod.2010.03.039.

761 (60) Scherzer, J.; Gruia, A. J. *Hydrocracking science and technology*, Chemical industries, Vol.  
762 66; Marcel Dekker, 1996.

763 (61) B.D. Muegge and F.E. Massoth. Basic studies of deactivation of hydrotreating catalysts with  
764 anthracene. *Fuel Processing Technology* 1991 (29), 19–30.

765

